2018

Experimental Design and Laboratory Characterization of a Medium- and High-Efficiency Rooftop Unit for use in Building Energy Simulations

Grant Wheeler
National Renewable Energy Laboratory, GRANT.WHEELER@NREL.GOV

Eric Kozubal
National Renewable Energy Laboratory, eric.kozubal@nrel.gov

Ron Judkoff
National Renewable Energy Laboratory, ron.judkoff@nrel.gov

Experimental Design and Laboratory Characterization of a Medium- and High-Efficiency Rooftop Unit for use in Building Energy Simulations

Eric Kozubal[1], Grant Wheeler[2], Ron Judkoff[3]

[1] National Renewable Energy Laboratory
Golden, CO 80401
303-384-6155
eric.kozubal@nrel.gov

[2]National Renewable Energy Laboratory
Golden, CO 80401
303.275.4577
Grant.wheeler@nrel.gov

[3]National Renewable Energy Laboratory
Golden, CO 80401
303-384-7520
ron.judkoff@nrel.gov

ABSTRACT

Commercial rooftop units (RTUs) that incorporate variable-speed components are quickly entering the marketplace; however, the design and modeling tools that calculate the energy benefits of these units cannot properly estimate performance. This is because 1) there are insufficient measured performance data of real systems that can be input into these simulations, and 2) building energy simulators are unable to properly interpret performance data. Therefore, publicly available data sets designed to encompass the entire performance map coupled with control sequence information are needed as inputs for these modeling programs to accurately estimate energy savings and promote the benefits of variable-speed RTUs. As part of the Validation and Uncertainty Characterization for Energy Simulation project funded by the U.S. Department of Energy, the National Renewable Energy Laboratory recorded and published data across the entire performance range for two commercially available RTUs: one with a two-stage compressor and variable-speed supply fan and another with a fully variable-speed compressor, supply fan, and condenser fan. This paper details 1) how the design of experiments was created and 2) the operational limitations of the two units that complicate the measurement and interpretation of the performance maps. This paper also discusses methods for improving energy simulation programs to properly interpret these data sets and integrate them into building energy simulation models.

1. INTRODUCTION

A challenge facing building energy modelers is the scarcity of data and performance maps for packaged heating, ventilating, and air-conditioning (HVAC) systems. This is especially true for smaller systems in the range of 5–30 tons because they are too small to merit specialized engineering assistance from manufacturers. Thus, most modelers must use either the default generic curves available within whole-building simulation computer programs or maps or curves that are extrapolated from commonly available ratings, such as the seasonal energy efficiency ratio (SEER) or integrated energy efficiency ratio (IEER). These modeling approaches are a relic of simpler equipment and create inaccuracies with today's modern systems that have nonintuitive performance characteristics and control sequences. Modern variable equipment is unlikely to be well modeled by either of these approaches, both of which evolved when most equipment was single speed. To address this issue and create generic performance maps typical of newer variable equipment, the National Renewable Energy Laboratory (NREL) fully characterized two rooftop units (RTUs)—a 5-ton/SEER 17 (RTU 1) and a 6-ton/IEER 23 (RTU 2)—with the purpose of developing comprehensive performance maps suitable for use with whole-building energy simulation computer programs. The SEER 17 contained a two-stage scroll compressor with R-410A, single-speed condenser fan, direct-drive variable-supply air fan with a high-efficiency motor, low leak dampers, hot gas reheat humidity control, and an economizer. The IEER 23 contained a variable-

speed direct-drive compressor, variable-speed fans, and control logic that maintained the compressor and thermal expansion valve (TXV) within their performance limitations. The steady-state performance data from these units were tabulated with the caveat that 1) there are significant constraints on how to interpret the data, and 2) the time-variant performance is not captured.

Tabularized performance maps are attractive because they facilitate downstream processing (often in the form of multidimensional curves) while maintaining the integrity of the original data. At least two initially independent groups have identified tabularized performance maps as the preferred way to store the data. The first is ASHRAE Standard Project Committee 205, *Standard Representation of Performance Simulation Data for HVAC&R and Other Facility Equipment.* This standard is being developed to encourage manufacturers to provide more extensive data and to make it easier for simulation programs to use the data. The second is the U.S. Department of Energy Technology Performance Exchange (TPEX), which is linked to the OpenStudio platform (NREL, 2018); however, in this project, we observed that the newest generation of variable equipment might require modifications to the tabularized construct.

2. BACKGROUND

This effort was part of a larger project sponsored by the Department of Energy's Building Technologies Office to provide empirical data for the validation of whole-building energy simulation computer programs. The end goal is to add empirical validation test suites to ANSI/ASHRAE Standard 140, *Method of Test for the Evaluation of Building Energy Analysis Computer Programs* (ASHRAE, 2017). The methodology underpinning Standard 140 consists of three kinds of tests: analytical, comparative, and empirical (Judkoff & Neymark, 2006). Currently, the standard is populated with several analytical and comparative test suites, but it lacks empirical tests (Judkoff & Neymark, 1995). This project had two purposes: the first was to develop empirically derived performance maps suitable for energy modeling using NREL's HVAC test facility; and the second was to use these maps in an update of two NREL reports, known as the HVAC BESTEST Volume 1 (Neymark & Judkoff, 2002) and Volume 2 (Neymark & Judkoff, 2004), which form the technical foundation of Standard 140 Section 5.3. The remainder of this paper describes the NREL effort to develop comprehensive performance maps for a 5-ton SEER 17 and a 6-ton IEER 23 RTU.

3. APPROACH

3.1 Design of Experiments

To characterize the entire performance map for both RTUs, a design of experiments (DOE) needed to be developed. A mixed-central composite design of experiments (MCC-DOE) was chosen rather than a complete full factorial design because of the large performance space for each unit. This is commonly seen in many DOEs where, because of the size of the full factorial design, an alternative design must be chosen to characterize the system (NIST, 2017)."Mixed" refers to the independent variables that were noncontinuous, such as wet and dry coil or compressor speed. Compressor speed was stated as a noncontinuous variable because it was either first or second stage, which corresponds to 67% and 100% volumetric capacity, for the first RTU or 25%, 50%, 75%, and 100% rotational speed (or volumetric capacity) for the second RTU. Separating the compressor speed into four distinct speeds (compressor stages) increased the number of tests; however, this was necessary because of the nature of the compressor performance map, which restricts maximum speed at several levels of compressor lift.

Table 1 shows the independent continuous variables for each RTU and each state of operation. RTU 1 had four discrete levels, one for each combination of wet/dry coil and two compressor stages. Similarly, RTU 2 had eight discrete levels. For each discrete level, an MCC-DOE test matrix was performed. The wet coil DOEs for RTU 1 and RTU 2 used different indoor air conditions as independent variables (dew point versus wet-bulb). Wet-bulb temperatures were used in RTU 2 because the MCC-DOE better covered the useable range of operation on a psychrometric chart; however, both MCC-DOE designs produced similarly shaped maps for interpolation.

The psychrometric and airflow boundaries were determined by the minimum and maximum expected values for a building: 15°C < $T_{ID,DB}$ < 35°C, 12°C < $T_{OD,DB}$ < 52 °C, and 4°C < $T_{ID,DP}$ < 28°C. Additionally, standard airflow per capacity was typically maintained between 42–60 l/s-$kW_{thermal}$ (320–450 CFM/t), which is typical of supply air flow rates. In the case of RTU 2, fan speed minimum was reached at 50% capacity, thus the airflow per kilowatt of capacity increased as compressor speed was reduced below 50%. RTU 2 reached as high as 110 l/s-$kW_{thermal}$.

Table 1: Continuous variables for each design of experiments

RTU 1: Wet Coil (Two Compressor Stages)	**RTU 1: Dry Coil (Two Compressor Stages)**	**RTU 2: Wet Coil (Four Compressor Stages)**	**RTU 2: Dry Coil (Four Compressor Stages)**
Indoor dewpoint ($T_{ID,DP}$)	Indoor dry bulb ($T_{ID,DB}$)	Indoor wet-bulb ($T_{ID,WB}$)	Indoor dry bulb ($T_{ID,DB}$)
Dewpoint depression ($T_{ID,DB} - T_{ID,DP}$)		Wet-bulb depression ($T_{ID,DB} - T_{ID,WB}$)	
Outdoor dry bulb ($T_{OD,DB}$)	Outdoor dry bulb ($T_{OD,DB}$)	Outdoor dry bulb ($T_{OD,DB}$)	Outdoor dry bulb ($T_{OD,DB}$)
Air mass flow rate (MFR_{SA})	Air mass flow rate (MFR_{SA})	Compressor lift (SCT – SST)	Compressor lift (SCT – SST)

Looking further into the boundaries for wet and dry tests, as well as for different stages, Table 2 and Table 3 show the limits for each DOE. When the system limitations prevented reaching the desired minimum or maximum, the component limitations were used instead. This case happened often when testing RTU 2 because of compressor and TXV limitations.

Table 2: RTU 1 boundaries for each DOE [°C]

	Compressor Stage	**$T_{ID,DB}$**		**$T_{OD,DB}$**		**$T_{ID,DP}$**		**$T_{ID,DP}$ Depression**	
		Min	Max	Min	Max	Min	Max	Min	Max
Wet	Stage 1	15	35	18	35	4	28	3	15
	Stage 2	21	35	23	52	9	25	3	20
Dry	Stage 1	20	35	12	35				
	Stage 2	19	35	13	52				

Table 3: RTU 2 boundaries for each DOE [°C]

	Compressor Speed	**$T_{ID,DB}$**		**$T_{OD,DB}$**		**$T_{ID,WB}$**		**$T_{ID,WB}$ Depression**	
		Min	Max	Min	Max	Min	Max	Min	Max
Wet	25%*	18	22	18	27	16	20	1	2
	50%	22	27	13	32	18	21	2	8
	75%	22	31	13	42	18	22	2	10.5
	100%	23	34	21	52	18	24	2	11.1
Dry	25%	20	27	18	27				
	50%	27	34	17	39				
	75%	27	35	17	42				
	100%	27	35	18	49				

*A Box-Behnken DOE was performed for RTU 2 at 25% because of the small operational space.

The wet tests were bounded by the dewpoint depression; if too large, it would result in a dry coil. The dewpoint depression criteria for wet coil operation is a function of airflow per capacity. As a result, RTU 2 running at 25% capacity has a dry coil when $T_{ID,DB} > 22$°C. The MCC-DOE also accounted for the saturated temperatures, as shown in Figure 1, which plots the predicted saturated evaporating dewpoint temperature (SST) and saturated condensing dewpoint temperature (SCT) along with the compressor's operational boundaries. Zones 1 through 3 defined the allowable compressor speed: Zone 1 (60%–100%), Zone 2 (27%–100%), and Zone 3 (20%–100%). Zone 4 is a special case, whereby the unit's operation at 25% capacity is constrained by the TXV. In this zone, the TXVs ability to meter refrigerant is restricted by the pressure difference across the valve. The last constraint applied was the system's maximum allowable outdoor air temperature (52°C), which affected the maximum SCT for the 100% DOE. The MCC-DOE design pattern for RTU 2 was primarily done using SCT and SST as variables, which is discernable in these plots.

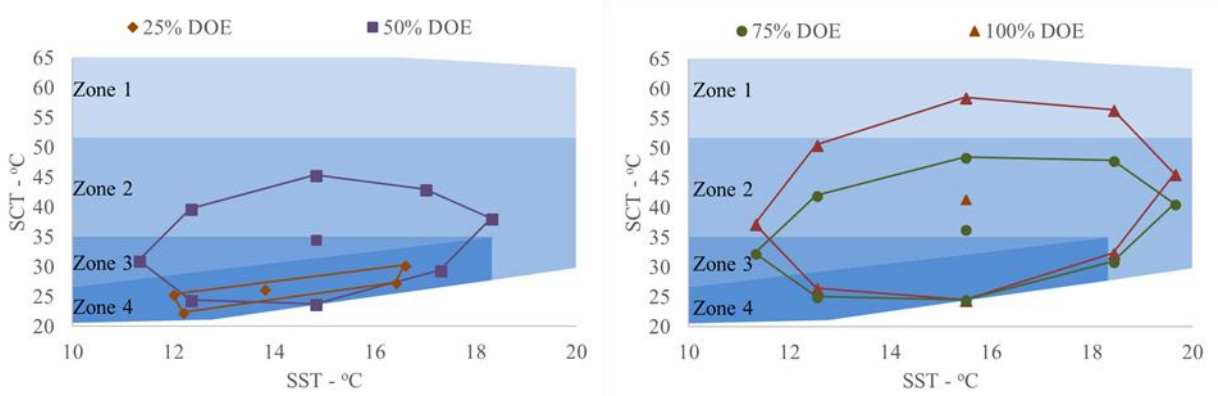

Figure 1: DOE for 25% and 50% compressor speeds (left) and for 75% and 100% compressor speeds (right)

3.2 Laboratory Setup

The laboratory apparatus was configured to supply three independently controlled airstreams to the experimental test stand and to accept three independently controlled return airstreams (Figure 3). The laboratory conditions the airstreams to the correct mass flow, temperature, and humidity using:

1. Dry bulb using Type T thermocouples: ±0.4°C/±0.25°C absolute/delta-temperature accuracy
2. Dewpoint using chilled mirror hygrometers: ±0.15°C/±0.05°C absolute/delta-dewpoint accuracy
3. Airflow using ASME low beta flow nozzle array: ±2% of mass flow reading accuracy
4. Ambient pressure: ±0.15% of reading
5. Airstream delta static pressure: ±5 Pascal accuracy

Other laboratory measurements included:

1. Condensate flow rate using Coriolis flow meter: 0.1% of reading
2. Power readings: 0.2% of reading (unit power, compressor, blower fan, condenser fan)
3. Refrigerant pressures: 0–6.87 MPa, ±0.25% of full scale (suction, discharge, liquid line)
4. Refrigerant temperatures: Type T thermocouples ±0.4°C (Compressor suction, discharge, middle of condenser, middle of evaporator)
5. Special measurements for RTU 2:
    a. Compressor speed (0–10 VDC, signal tap)—maximum 4,500 RPM
    b. Supply fan speed (0–10 VDC, signal tap)—measured range: 1,118–2,523 SCFM
    c. Condenser fan speed (laser tachometer on fan hub)—maximum 1,000 RPM

Dewpoint and dry bulb temperature were controlled to the set point within ±0.3°C and ±0.2°C. Airmass flow rates were controlled to ±1% of flow stability. The ventilation dampers on each system were sealed/taped shut to avoid small air leaks from the outdoor plenum to the inlet to the evaporator coil. This was done because performance maps are expected to represent the performance at the known evaporator inlet condition; however, crevices in the RTU cabinets' construction and hatches allowed minute air leakage. Further, the combined air leak flow rate through crevices around hatches and dampers (when closed) were measured to be as high as 5% depending on the air pressure in the indoor air duct. As a result, these units provide up to 5% (potentially) unintended ventilation airflow when dampers are shut.

RTU 1 was controlled using staged thermostat signals to control capacity. RTU 2 was controlled using a fictitious indoor temperature signal fed to the indoor temperature thermistor input. The laboratory control system maintained the proper measured compressor speed by varying the thermistor signal using a proportional-integral controller. These load control techniques ensured that the normal operational control logic of the RTUs was enabled.

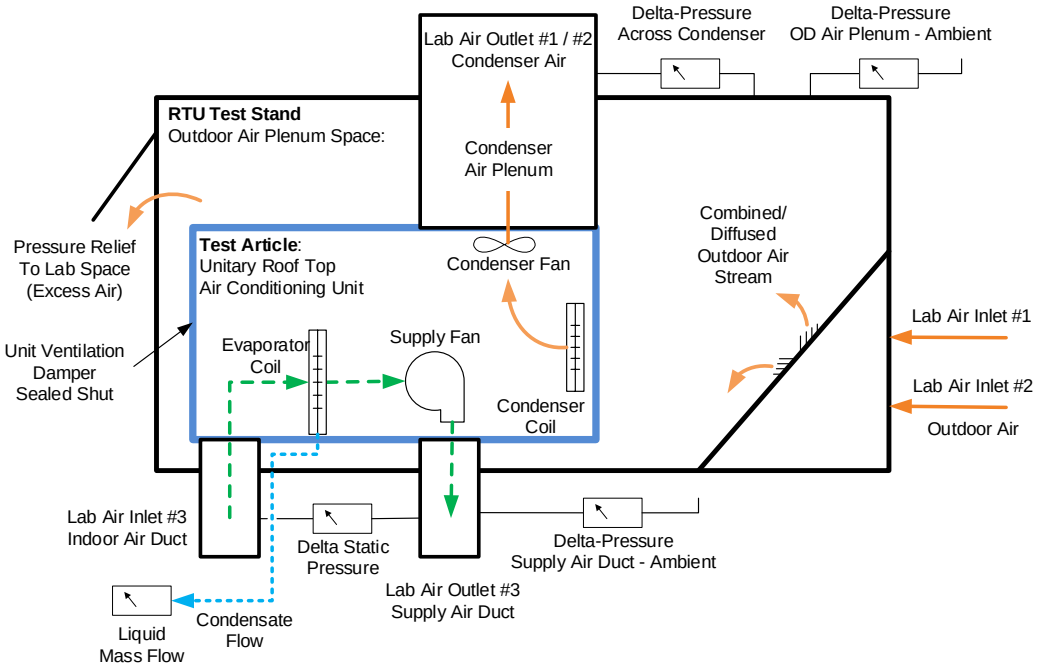

Figure 3: Schematic of airstreams through RTU, plenums, and ducts

Using the RTU cabinet as a control volume, power, supply airflow, and moisture removal balances were calculated using equations 1 through 3 with power and supply air mass balances for all data, as summarized in Table 4. When the enthalpy difference between the outdoor air and indoor air was similar, the power balance was typically 1.00 ± 0.02. The measured values outside this range are thought to be from the cabinet air leaks and heat conduction through the cabinet. The dry-coil air-side moisture removal rate was measured to be less than ±0.15 kg/h. Periodic wet-coil checks between the air-side and liquid condensate measurements were within ±0.15 kg/h.

$$Unit\ power\ balance = \left(\frac{Capacity_{total} + Power_{unit\ total}}{Heat_{rejected\ by\ condenser}}\right) \quad (1)$$

$$\text{Supply air mass balance} = \left(\frac{MFR_{evap\ in}}{MFR_{evap\ out}}\right) \quad (2)$$

$$\text{Moisture removal balance} = \left(\frac{MFR_{airside\ moisture\ removal}}{MFR_{condensate\ measurement}}\right) \quad (3)$$

Table 4: Measured power and evaporator air mass flow balances for all data points taken

	RTU 1 AVERAGE (RANGE)	**RTU 2 AVERAGE (RANGE)**
UNIT POWER BALANCE	0.99 (0.94–1.05)	1.02 (0.97–1.08)
EVAPORATOR AIR MASS BALANCE	0.99 (0.97–1.03)	1.00 (0.99–1.01)

Test duration was dependent on the individual unit's operation at each psychrometric condition. If unit operation was steady, the data were collected for 30 minutes while the power balance and latent capacity were steady to within ±0.01 and ±0.15 kg/h. Both RTU 1 and RTU 2 exhibited non-steady behaviors. RTU 1 turned on the reheat coil for 3 minutes every 90 minutes. The reheat coil caused 1) a decrease in total cooling and 2) a large decrease in latent cooling because condensed water on the reheat coil was evaporated into the supply air during this cycle. RTU 2 operation less than 55% compressor speed had periodic changes in operation. The system ramped the compressor up to 55% for about 1½ minutes every 20 minutes. This cycle also occurred as the compressor first turned on and as it prepared to turn off. This time-variant operation affects real-life performance; for example, if a building load requires 25% capacity for 10 minutes, this unit will provide capacity at 55% for 5 minutes and then shut off. The

blower and condenser fan speeds also ramped during these periods (Figure 4). In the figure, the quasi-steady-state performance was used (from start to finish lines) and had an average compressor speed of 22.8%. The time period selected was exactly 40 minutes to capture two full 20-minute cycles. Note that the 20-minute cycles are not identical but similar. Gathering sequential, identical cycles was not possible; however, small changes in compressor speed were determined to have little effect on efficiency (COP). The target speeds were 25%, 50%, 75%, or 100% ± 2% compressor speed; however, exceptions were made for IEER measurement. For example, the 25% IEER point required the compressor to run at 23% speed to achieve 25% ± 3% of full load air-side total capacity (AHRI, 2015).

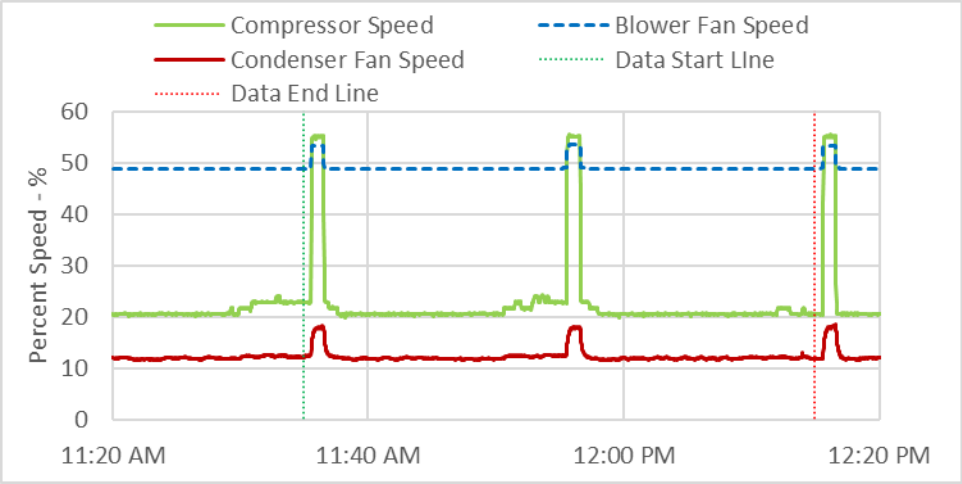

Figure 4: Example component speed when operating at an average of 23% compressor capacity

Figure 5 shows the inlet and outlet dewpoint during the same test point. During the short periods when the compressor ramped up, the evaporator coil provided some dehumidification; however, the water removed was re-evaporated after the compressor ramped back down to nominal speed. The net sensible heat ratio was 1.00.

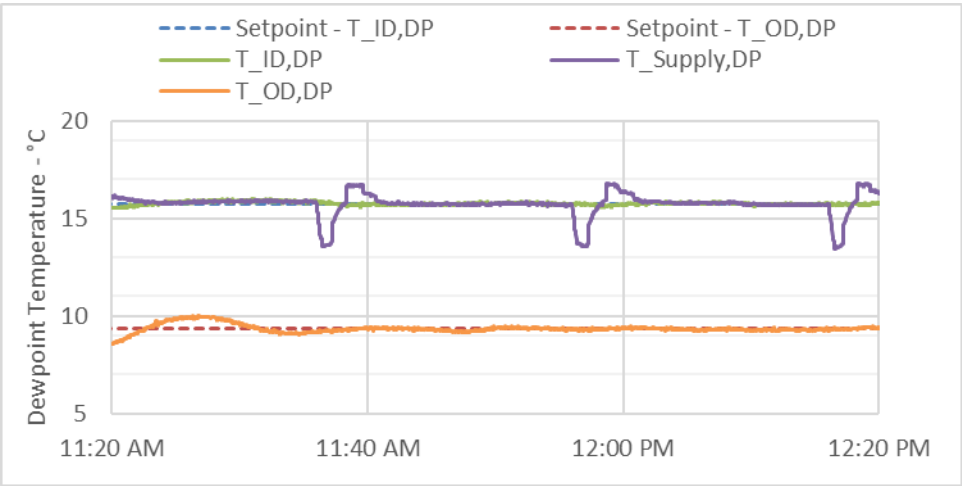

Figure 5: Example outlet dewpoint temperatures during the same test as shown in Figure 4

3.3 Adjustments for Elevation

Laboratory methods and calculations conformed to ASHRAE Standard 37-2009 (ASHRAE, 2009); however, the laboratory is 1,783 meters above sea level elevation. Because sea level performance is desired, modification to typical procedures were implemented. The following criteria are necessary conditions to enable performance correction between altitude and sea level performance: 1) mass flow rates across the evaporator coil and condenser coils must be equal to that at sea level, and 2) the entering evaporator dry bulb and relative humidity must be equal to sea level conditions. The second criteria ensures that the dewpoint depressions ($T_{ID,DB} - T_{ID,DP}$) are the same between Golden, Colorado, (altitude) and sea level conditions. Given these criteria, the effectiveness of the

evaporator and condenser coils will be equal between altitude and sea level conditions. This is a result of the effectiveness of the finned coils being solely dependent on the number of transfer units (NTUs).

$$NTU_{finned\ coil} = \left(\frac{\mathrm{U} \cdot \mathrm{A}}{MFR_{air,evap} \cdot C_{p,air}}\right)_{finned\ coil} \tag{4}$$

For internal flows, the overall heat transfer coefficient (U) is solely a function of mass flow rate. Thus, maintaining equal mass flow ensures that the NTU and effectiveness are equal between altitude and sea level. As a result, the supply air temperature of a dry coil, SST, and SCT will be also be identical at altitude and sea level.

When the evaporator coil is wet (providing dehumidification), then a small additional adjustment is required to calculate outlet conditions at sea level from those measured at altitude. Equation 5 is applied, which asserts that the refrigeration capacity is unchanged, thus the air-side capacity is equal between altitude and sea level. Applying Equation 6 is the result of the evaporator coil effectiveness remaining unchanged.

$$Air\ enthalpy\ change\ across\ evaporator: \delta h_{evap,SL} = \delta h_{evap,alt} \tag{5}$$

$$Evaporator\ air\ outlet: RH_{SL} = RH_{alt} \tag{6}$$

However, this wet coil correction introduces a small error in capacity and compressor power because the SST at altitude will be slightly more than that at sea level because of the increased evaporator moisture removal capacity at altitude. This phenomenon is because of the slope of the psychrometric saturation line is steeper at higher elevation. For the data presented in this paper, the error in SST was calculated to be less than 0.7°C, which results in a 1% average error in the measured compressor's temperature lift (and resultant power) across all data points taken.

Both RTUs controlled to the proper supply air mass flow rate. Thus, the internal static pressure drops were higher by the ratio of sea level to altitude ambient pressures. To properly correct the fan power, the sea level nominal static pressure across the supply inlet to supply outlet was set to 50 Pa and 62 Pa (for RTU 1 and RTU 2) and adjusted for measured ambient pressure as shown in Equation 7. The supply fan power was then adjusted to sea level performance (Equation 8), which is derived from fan laws.

$$\delta SP_{alt} = VFR_{air,evap\ out}\delta SP_{SL}\left(\frac{101325\ \mathrm{Pa}}{P_{ambient}}\right) \tag{7}$$

$$W_{SF,SL} = W_{SF,alt}\left(\frac{P_{alt}}{101325\ Pa}\right) \tag{8}$$

The condenser volumetric airflow rate was characterized versus rotational speed. Condenser air mass flow rate was boosted using the laboratory fans during the tests using Equation 9. The condenser fan power was adjusted using fan law correlations from the characterized flow relationship.

$$VFR_{cond.,test} = VFR_{cond,characterized}\left(\frac{14.7\ psi}{P_{ambient}}\right) \tag{9}$$

3.4 Verification of Experimental Accuracy

As a final step to ensure proper calculations and laboratory setup, the AHRI Standard 340 rating conditions (AHRI, 2015) were compared to the measured values. Standard rated values are the accepted measurement for system net capacity, energy efficiency ratio (EER), and IEER. The error shown is acceptable per the AHRI 210 and 340 Standards (AHRI, 2008 & AHRI, 2015), which accounts for manufacturing variability.

Table 5: Relative performance to standard rated performance as verification step for laboratory setup

	RTU 1	**RTU 2**
Measured capacity/standard rated capacity	102%	98%
Measured EER/standard rated EER	95%	101%
Measured IEER/standard rated IEER	-	101%

3.5 Data Output

The outputs also needed to meet the minimum TPEX requirements for performance maps, which are shown in Table 6. This resulted in 71 and 97 measured test sets for RTU 1 and RTU 2 with the 10 variables displayed in Table 6 that were uploaded and are publicly available in the TPEX website (NREL, 2018).

Additionally, statistical analysis software was used to determine the significant variables, which resulted in empirical polynomial models. Twelve and 24 models were created for RTU 1 and RTU 2 to fully define their performance. We used least squares regression with the same set of TPEX variables to predict dependent variables to within 5% error. Publishing the variables and their coefficients is too voluminous for this paper but is available via the TPEX website. The models for each RTU were then used to create a spatially even, full factorial set of performance data points that were also then entered into the TPEX database. Table 6 shows the TPEX variable list, with dependent variables calculated from the empirical models.

Table 6: List of TPEX data variables. Dependent variables were calculated from the models derived for each.

TPEX Data Requirements	RTU 1	RTU 2
$T_{ID,DB}$	Independent	Independent
$T_{ID,WB}$	Independent	Independent
$T_{OD,DB}$	Independent	Independent
MFR_{SA}	Independent	Dependent
Supply fan power	Dependent	Dependent
Static pressure	Independent	Independent
Gross cooling capacity	Dependent	Dependent
Gross sensible heat ratio	Dependent	Dependent
Gross power	Dependent	Dependent
Stage/compressor speed	Independent	Independent

As discussed earlier, RTU 1 maintained the set supply air mass flow rate, and RTU 2 varied the supply air mass flow rate to supply air at near constant temperature for compressor speed more than 50% and at constant airflow for compressor speed less than 50%. Building energy simulation tools, such as EnergyPlus, typically disaggregate refrigeration and supply fan control algorithms, and it is incumbent upon the building simulation user to input the correct control associations that link refrigeration capacity and supply air fan speed (energyplus.net, 2018). Further, EnergyPlus uses three psychrometric inputs to define the RTU capacity and power: $T_{ID,WB}$, $T_{OD,DB}$, MFR_{SA}; whereas $T_{ID,DB}$ was shown to be a significant variable to define performance.

To meet a building energy simulation's thermal and latent loads, EnergyPlus also interpolates between stages or compressor speeds to determine performance; however, RTU 2 clearly shows that this algorithm would fail because the operational space is limited for each speed. As an example, the simulation might erroneously interpolate between 25% and 50% speeds in a space were 25% speed will not run (e.g. $T_{ID,DB} > 22°C$). In this case, the unit would instead cycle. To further complicate the issue, cycling operation is constrained to the start-up/shutdown sequencing of the unit, such that 55% capacity would be used for a portion of the cycling behavior.

6. CONCLUSIONS

A method of creating performance maps using MCC-DOE was used to characterize two modern RTUs. These units were tested at an elevation of 1,783 m (81.7 kPa std. pressure), and a proposed method for adjusting the performance to sea level pressure was applied. The characterized RTUs resulted in 71 and 97 measured data sets. A second, full factorial, evenly spaced data set was derived using statistical software, and this created empirical models of key dependent variables. Interpolated data sets were developed based on the empirical models to provide tabular results. The measured and full factorial data sets were all uploaded on a publicly available website.

To properly use the publicly available data sets for advanced RTU modeling, building energy simulation tools require the ability to properly interpret which models to use based on limitations of the systems' operational ranges and onboard control strategies. Further, time-variant operations of these RTUs are not incorporated into these performance maps. This represents a challenge for existing building simulation programs, which are not inherently set up to handle the complex logic required to properly predict performance.

The variable-speed RTU particularly requires careful attention to understand the limitations for each compressor speed as it pertained to input psychrometric conditions. Real operation of high temperature at low capacity results in cycling of the refrigeration system rather than steady-state operation at a lower speed. These operational characteristics are the result of the manufacturer's choice of compressor and TXV combination. Other manufacturer's component choices will likely require an in-depth study, such as was done in this report, to determine the operational characteristics.

Future work will focus on how to better incorporate the advanced controls of these modern RTUs into building energy simulation programs. One such method will be to investigate a co-simulation modeling approach that uses time-variant control algorithms in combination with a tabulated performance map to properly output the performance. The control algorithm would account for start-up/shutdown sequences and limitations because of internal component specifications. This method could be programmed and publicly provided as stand-alone code to be incorporated or co-simulated with building energy simulation programs. As additional air conditioners are characterized, a library of co-simulation code sets would be available to the energy modeling community.

NOMENCLATURE

Variables

A	area	m^2
C_p	constant pressure specific heat	kJ/kg-°C
DOE	design of experiments	-
δh	enthalpy change	kJ/kg
δSP	delta static pressure	Pascal (Pa)
EER	energy efficiency ratio	Btu/W-h
IEER	integrated energy efficiency ratio	Btu/W-h
MCC-DOE	mixed central composite design of experiments	-
MFR	mass flow rate	kg/s
NTU	number of transfer units	-
P	pressure	Pascal (Pa)
RH	relative humidity	%
RTU	rooftop unit	-
SCT	saturated condensing dewpoint temperature converted from R410A pressure measurements (F-Chart Software, 2018)	°C
SST	saturated evaporating dewpoint temperature converted from R410A pressure measurements (F-Chart Software, 2018)	°C
T	temperature	°C
TXV	thermal expansion valve	-
U	overall heat transfer coefficient	kW/ m^2-°C
VFR	volumetric flow rate	liters/s
W	work	kW

Subscript

alt	at measured altitude pressure
ambient	ambient conditions
cond	condenser
evap	evaporator
DB	dry bulb
DP	dewpoint
ID	indoor
OD	outdoor
SA	supply air
SF	supply fan
SL	sea level
WB	wet-bulb

REFERENCES

AHRI. (2008). *ANSI/AHRI Standard 210/240: Performance Rating of Unitary Air-Conditioning & Air-Source Heat Pump Equipment.* Arlington.

AHRI. (2015). *AHRI Standard 340/360-2015: Performance Rating of Commercial and Industrial Unitary Air-conditioning and Heat Pump Equipment.* Arlington, VA: Air-Conditioning, Heating, and Refrigeration Institute.

ASHRAE. (2009). *ANSI/ASHRAE Standard 37-2009: Methods of Testing for Rating Electrically Driven Unitary Air-Conditioning and Heat Pump Equipment.* Atlanta, GA: ASHRAE.

ASHRAE. (2017). *ANSI/ASHRAE Standard 140-2017: Standard Method of Test for the Evaluation of Building Energy Analysis Computer Programs.* Atlanta, GA: ASHRAE.

ASHRAE, S. (n.d.). Standard Representation of Performance Simulation Data for HVAC&R and Other Facility Equipment.

energyplus.net. (2018, 04 30). Retrieved from https://energyplus.net/sites/default/files/pdfs/pdfs_v8.3.0/InputOutputReference.pdf

F-Chart Software. (2018). *Engineering Equation Solver v10.305 (Professional).*

Judkoff, R., & Neymark, J. (1995). *International Energy Agency Building Energy Simulation Test (BESTEST) and Diagnostic Method.* NREL/TP-472-6231.

Judkoff, R., & Neymark, J. (2006). Model Validation and Testing: The Methodological Foundation of ASHRAE Standard 140. *ASHRAE Transactions* (pp. 367-376). Quebec City, Canada: ASHRAE.

Neymark, J., & Judkoff, R. (2002). *International Energy Agency Building Energy Simulation Test and Diagnostic Method for Heating, Ventilating, and Air-Conditioning Equipment Models (HVAC BESTEST); Volume 1: Cases E100-E200.* NREL/TP-550-30152.

Neymark, J., & Judkoff, R. (2004). *International Energy Agency Building Energy Simulation Test and Diagnostic Method for Heating, Ventilating, and Air-Conditioning Equipment Models (HVAC BESTEST): Volume 2: Cases E300-E545.* NREL/TP-550-36754.

NIST, S. (2017, May 14). *e-Handbook of Statistical Methods*. Retrieved from Central Composite Designs: https://www.itl.nist.gov/div898/handbook/pri/section3/pri3361.htm

NREL. (2018). *Technology Performance Exchange (TPEX)*. Retrieved from NREL HVAC Lab: https://www.tpex.org/company/49221/products

Acknowledgments

This work was authored in part by Alliance for Sustainable Energy, LLC, the manager and operator of the National Renewable Energy Laboratory for the U.S. Department of Energy (DOE) under Contract No. DE-AC36-08GO28308. Funding provided by the U.S. Department of Energy Building Technologies Office is gratefully acknowledged. We also express our gratitude to Amir Roth of the U.S. Department of Energy for invaluable support and guidance in the conduct of this work. The views expressed in the article do not necessarily represent the views of the DOE or the U.S. Government. The U.S. Government retains and the publisher, by accepting the article for publication, acknowledges that the U.S. Government retains a nonexclusive, paid-up, irrevocable, worldwide license to publish or reproduce the published form of this work, or allow others to do so, for U.S. Government purposes.

Notice